Paper Number 223

Loosely-Coupled Multibody Dynamics/CFD Analysis for a Rotor in Descending Flight

Jae-Sang Park*, Jeong-Hwan Sa, Young-Hyun You, Sung Nam Jung, and Soo-Hyung Park

Department of Aerospace Information Engineering,
Konkuk University, Seoul, KOREA

Abstract

This paper conducts the coupled analysis using the rotorcraft computational structural dynamics (CSD) based on the nonlinear flexible multibody dynamics and a computational fluid dynamics (CFD) to correlate the measured data of a rotor in descending flight. The nonlinear flexible multibody dynamics code, DYMORE, and a RANS (Reynolds Averaged Navier-Stokes) CFD solver, KFLOW, are used for a loosely-coupled analysis with the delta-airloads method. The three test cases of the HART (Higher-harmonic Aeroacoustic Rotor Test) II -baseline, minimum noise, and minimum vibration- are considered for the present correlation study of the blade-vortex interaction (BVI) airloads, rotor trim, blade deformations, blade structural loads, and rotor wakes. The predictions by DYMORE analysis alone with the freewakes, DYMORE/KFLOW coupled analyses using the isolated rotor and rotor-fuselage models are compared with the measured data. As compared to DYMORE analysis alone and the coupled analysis with the isolated rotor model, the coupled analysis using the rotor-fuselage model shows an excellent prediction of M^2C_n in the phase and BVI loadings, particularly for the baseline case and it also improves the trimmed cyclic pitch control angles. The blade deformations, structural loads, and wake positions are predicted fairly or well by both the coupled analyses using the isolated rotor and rotor-fuselage models. In addition, the predictions of the elastic twist deformation in the baseline case and the flap bending moments in all the three cases are considerably improved by the coupled analyses than the result by DYMORE analysis alone.

Introduction

The blade vortex interaction (BVI) is caused by interaction between the rotor blades and their trailed vortices. This BVI phenomenon occurs mainly in descending flight and low speed transition flight and causes significant noise and/or vibration problems. In order to improve basic understanding on the formation of vortex wakes and their interaction leading to noise and vibration, an international cooperative program HART II was conducted in 2001 [1], preceded the earlier HART I [2]. Through a series of wind tunnel tests, massive measurement data [3] was obtained for the noise level, airloads, vortex wakes, blade deformations, and structural loads, with and without higher harmonic pitch control (HHC) inputs.

Along with the HART II test, a significant volume of research have been conducted to validate the rotorcraft comprehensive analysis [4, 5] based on the computational structural dynamics (CSD), computational fluid dynamics (CFD, [6, 7]), and CSD/CFD coupled analyses [8-14]. The rotorcraft comprehensive analysis could predict reasonably the BVI airloads, but the prediction accuracy seriously depends on the selection of the empirical parameters for the wake modeling. The rotor CFD analysis also predicted the BVI phenomena well and it can overcome the limitations of the lifting line theory used in the rotorcraft comprehensive analysis, but the measured blade deformations should be prescribed to consider the elastic effect of the blade. Recent study [8] using a loose CSD/CFD coupling showed a promising outcome for the HART II validation. Specifically, the BVI airloads prediction capability was improved significantly, through combining the strengths of the CSD and CFD approaches. Recently, the fuselage model as well as the rotor system model has been introduced to the CFD modeling for the HART II [9-14], and the inclusion of a fuselage model improved the phase of the section normal force and the BVI loadings in the advancing side [11, 12].

Although the previous CSD/CFD coupled analyses were conducted successfully for the HART II, most research adopted CAMRAD II [15] as a rotor CSD code except for Refs. [13, 14]. In Ref. [14], a nonlinear flexible multibody dynamics code which has the powerful multibody modeling capability, DYMORE [16], was coupled with an unstructured CFD solver, FUN3D [17]. The BVI airloads, rotor trim, blade deformations, and blade structural moments, using a rotor-fuselage model, were correlated well with the measured data. However, only the baseline case without HHC input was investigated.

This work aims at performing a correlation study, against the measured data of the HART II rotor, using a loosely-coupling approach between the DYMORE and a RANS (Reynolds Averaged Navier-Stokes) CFD solver, KFLOW [7]. Not only the baseline (BL) case but the minimum

noise (MN) and the minimum vibration (MV) cases of the HART II rotor are considered. The fuselage is modeled in the CFD analysis for more realistic analysis. Predicted section normal force, rotor trim, blade deformations, blade structural loads, and vortex positions, obtained with and without a fuselage model, are correlated against the measured data.

Test Data

Description of the HART II test

The HART II rotor was designed to match the rotating frequencies of the 1st, 2nd flap, 1st leadlag, and 1st torsion modes at the nominal rotor speed of the full-scale BO-105 rotor blade. A NACA23012 airfoil with a tab is used. The general properties [18] of the HART II rotor blade are summarized in Table 1.

Table 1 General properties of the HART II rotor [18]

Rotor type	Hingeless
Number of blades, N	4
Rotor radius, R	2.0 m
Location of feathering hinge	$0.0375R$
Chord length, c	0.121 m
Solidity, σ	0.0770
Airfoil section	NACA23012 mod
Blade built-in twist	-8.0˚ (Linear)
Precone angle	2.5˚
Nominal rotor speed, Ω_{ref}	109.0 rad/s

The HART II rotor was tilted by about 5.3˚ aft at DNW test and had a thrust level (C_T/σ) of 0.056 at an advance ratio μ of 0.15. In the present prediction, the wind tunnel wall model is not considered, thus the wall correction is applied, as a result the corrected shaft tilting angle is 4.3˚ for the rotor-fuselage model. For the isolated rotor model, the fuselage effect as well as the wind tunnel wall effect is considered, thus the corrected shaft tilting angle of 4.5˚ is used. The 3-per-rev (3P) pitch control inputs given in Table 2 were introduced for the minimum noise (MN) and minimum vibration (MV) cases.

Table 2 HHC pitch inputs for the MN and MV cases

Cases	θ_{3P}	ψ_{3P}
MN	0.81˚	300˚
MV	0.79˚	180˚

The pressure on the reference blade (blade No. 1) surface was measured at a single blade station (87% span) using the 17 pressure transducers distributed in the chordwise direction. The blade positions and deformations were measured optically by means of a stereo pattern recognition (SPR) technique. The blade structural loads were measured with the six strain gauges: three for the flap bending moments at r/R=0.15, 0.17, and 0.19, two for the leadlag bending moments at r/R=0.14 and 0.17, and one for the torsion moment at r/R=0.33. The rotor wake system including tip vortex geometry and vortex structures over the entire rotor disk was measured by a 3-component Particle Image Velocimetry (PIV) technique. All of the measured data except for the blade structural loads can be found in Ref. [3]. Therefore the measured values of the blade structural moments given in Ref. [11] are used for the present correlation.

Prediction methods

Nonlinear flexible multibody dynamics: DYMORE

The nonlinear flexible multibody dynamics, DYMORE, is used as a rotor CSD code for the present study. Although DYMORE has not been specially developed for the rotorcraft analysis, its powerful multibody modeling capability based on the arbitrary topology can represent the complex rotor control systems effectively. DYMORE has various multibody elements; rigid bodies, rigid and elastic joints and nonlinear elastic bodies such as beams, plates, and shells based on the finite element method. The geometrically exact beam theory [19] is used for the nonlinear elastic beam. Furthermore, DYMORE has simple aerodynamic models based on the lifting line theory for rotors and wings. As a rotor inflow model, the finite-state dynamic inflow model [20] is included originally in DYMORE. For the loosely-coupled analysis with a CFD, the finite-state dynamic inflow model is used through the iteration procedure, but the freewake model [21] which was newly implemented into DYMORE is used for the DYMORE analysis alone [5]. The autopilot theory is used to adjust the collective, lateral, and longitudinal cyclic pitch control angles to match the trim conditions.

In the present DYMORE modeling for the HART II rotor system, the four nonlinear elastic blades and a rigid hub are considered as shown in Figure 1. For the finite element modeling of the blade, each blade is discretized into 10 cubic beam elements. The blade section properties can be found in Ref. [18]. The equivalent torsional spring at the feathering hinge is used to represent the stiffness of the rotor control system. The value of the torsional spring constant is determined appropriately to match the first torsional frequency at the nominal rotor speed given in Ref. [18]. The hub is modeled as a rigid body and connected to a revolute joint with a prescribed rotational speed. For the aerodynamic loads on the blade, 31 airstations are used

with equal spacing on each blade. A C81 table for a NACA23012 airfoil with a tab is also utilized. In the freewake modeling for DYMORE analysis alone, the initial core radiuses at the root and tip of a blade use the values of 1.0c and 0.2c, respectively.

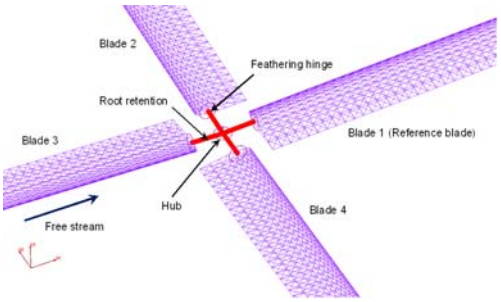

Figure 1 DYMORE modeling for the HART II rotor system

Navier-stokes CFD solver: KFLOW

The KFLOW [7] is a parallelized multi-block, structured, three-dimensional Navier-stokes CFD solver and is capable of computing time-accurate moving body problems by employing a Chimera overlapped grid system. A second-order accurate, dual-time stepping scheme combined with a diagonalized alternating directional implicit (DADI) method is used. The inviscid fluxes are calculated using the fifth-order weighted essentially non-oscillatory (WENO) scheme, while the central differencing technique is applied to the viscous fluxes. In the present calculation, the k-ω Wilcox-Durbin (WD+) model is used as a turbulence model. The moving overlapped Chimera grid system with the two different types of grids (blade and background grids) and the additional fuselage grids are used as shown in Figure 2. The C-mesh topology grids around a blade and O-type grids around the fuselage are created. The blade grids extend 1.5*c* from the blade surface in all directions. The blade grids are clustered near the leading edge, trailing edge, and blade tip regions. They are also clustered along the normal direction in the vicinity of the wall. The cell spacing for the first grid point from the wall boundary is $1.0\times10^{-5}c$. The background grids consist of an inner region that extends 4*c* above, 3*c* below from a blade, and 1.5*c* away from the blade tip. The inner region has a uniform spacing in all directions. The far field boundary is located 5 times larger than a blade radius *R* form the rotor hub. The background grids have a spacing of 0.1*c* for both the isolated rotor and rotor-fuselage models. Table 3 summarizes the grid system for the present CFD calculation which is selected based on the authors' previous works [7, 12] and Figure 3 shows the grid systems for the rotor-fuselage model.

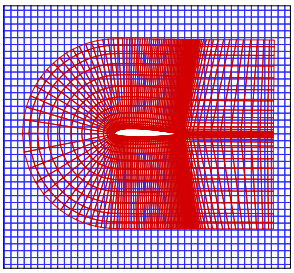

(a) Blade and background grids

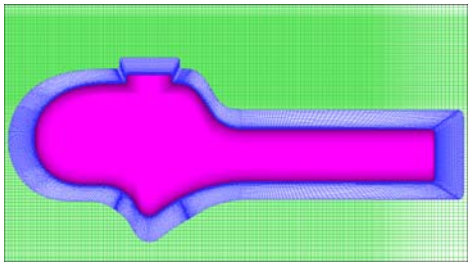

(b) Fuselage grids

Figure 2 Blade and fuselage grids

Table 2 Grid systems for DYMORE/KFLOW coupled analysis (M : Millions)

Grid type	Isolated rotor	Rotor-Fuselage
Background grid	111×401×401* (17.8 M cells)	161×449×401 (29.0 M cells)
Blade grid	321×97× 49† (1.53 M cells)	321×97×49 (1.53 M cells)
Fuselage grid	N/A	177×289×49 (2.51 M cells)
Total grid	23.95 M cells	37.60 M cells

* Vertical × lateral × longitudinal directions
† Chordwise × spanwise × normal directions

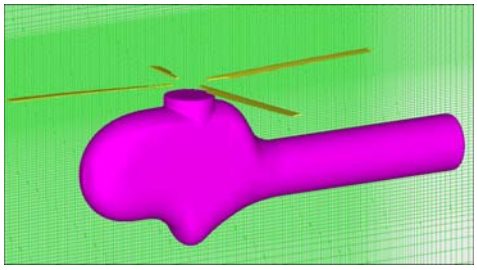

Figure 3 CFD grid systems for the HART II rotor-fuselage model

Loose coupling algorithm

The loosely-coupled analysis of DYMORE (CSD) and KFLOW (CFD) is performed by using the delta-airloads technique [22]. In this coupling strategy, DYMORE passes the trimmed pitch control angles and the blade elastic deformations such as the flap, leadlag deflections, and torsion deformation to KFLOW, while KFLOW passes the delta-airloads ($\Delta F/M$) defined as the difference between KFLOW airloads (F/M^{CFD}) and DYMORE's internal lifting line airloads (F/M^{LL}) using the finite-state dynamic inflow model to DYMORE. It is noticeable that the present DYMORE/KFLOW coupling algorithm uses the 6 components of the blade section airloads (3 forces and 3 moments) defined in the inertial frame while the previous rotor CSD/CFD coupling analyses using CAMRAD II usually use the two section forces (normal and chordwise forces) and one section moment (pitching moment) defined in the rotating frame. The data between the two codes is exchanged once per rotor revolution on a periodic basis. The loose coupling iteration is repeated until CFD airloads and pitch control angles are converged. All of the coupled analysis results in this paper are obtained through the 5 to 8 iterations. In the present coupled analysis, KFLOW uses the time step of 0.2˚ (1800 steps per one rotor revolution). In addition, the initial KFLOW run requires three rotor revolutions to establish the flow field and a periodic solution, whereas in the subsequent iterations, one and a quarter revolution is used. Figure 4 shows the DYMORE/KFLOW loose coupling algorithm.

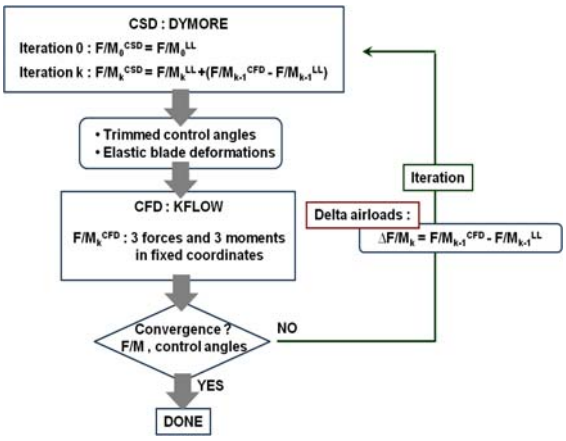

Figure 4 Flowchart for DYMORE/KFLOW loose coupling procedure (F/M = forces and moments)

Results and discussion

Airloads

Figures 5 to 7 show the correlations of the section normal force, M^2C_n, at r/R=0.87 between the predictions and measured data for the BL, MN, and MV cases. The prediction results are obtained by DYMORE analysis alone with the freewakes [5] and DYMORE/KFLOW coupled analyses using the isolated rotor and rotor-fuselage models. For the BL case given in Figure 5, DYMORE analysis with the freewake model predicts the BVI airloads well in the phase and the fluctuations of M^2C_n, although it misses the first two BVI events in the first quadrant. The coupled analysis with the isolated rotor model shows the reasonable prediction of the BVI loading however the significant phase lag phenomenon is observed at around the azimuth angle of 180˚ and some of BVI events in the first quadrant are not captured. On the contrary, the coupled analysis with the rotor-fuselage model shows a better prediction of BVI airloads since the number of and the fluctuation magnitudes of BVI events are predicted nicely in both the first and fourth quadrants. In addition, the phase of M^2C_n which is closely related to its lower harmonic components (less than 7-per-rev) [11, 12] is significantly improved as compared with the coupled analysis using the isolated rotor model. This is because the fuselage model has an effect on the rotor inflow distribution as a result, the mis-distance between the blade and vortices is also influenced [11, 12].

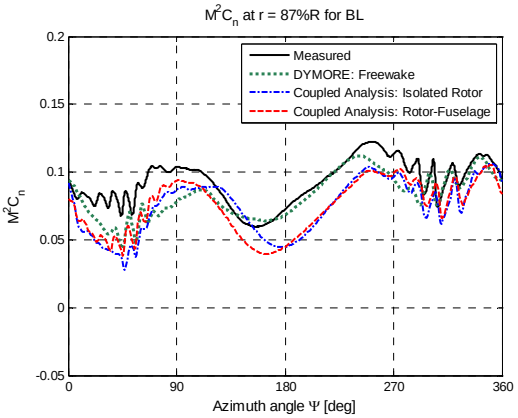

Figure 5 Correlation of M^2C_n at r/R=0.87 for the BL

Figure 6 shows the correlation of M^2C_n for the MN case. DYMORE with the freewakes predicts the BVI loading reasonably, but the fluctuation magnitude of M^2C_n in the retreating side is under-predicted moderately. Both the isolated rotor and rotor-fuselage models for the coupled analyses give good correlations in both advancing and retreating sides since they capture most of the BVI events. But the coupled analysis with the rotor-fuselage model improves the phase of M^2C_n slightly as compared to the coupled analysis with the isolated rotor model. The

correlation of M^2C_n for the MV case is given in Figure 7. DYMORE analysis alone captures well the fluctuations of M^2C_n caused by the BVIs in both the first and fourth quadrants but over-predicts the magnitude of M^2C_n in the second quadrant. As in the previous result for the MN case, the coupled analyses predict the BVI loading well however the rotor-fuselage model shows a better prediction since it improves the phase of M^2C_n slightly and captures all of the BVI events as compared to the coupled analysis using the isolated rotor model.

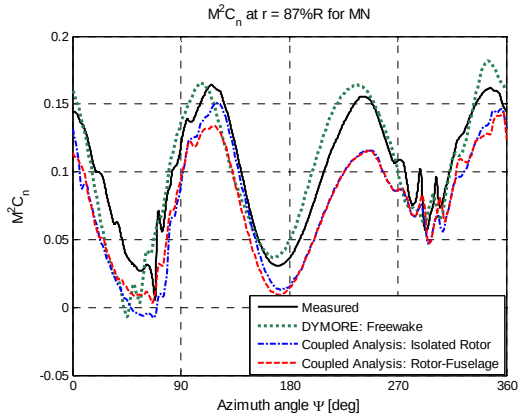

Figure 6 Correlation of M^2C_n at r/R=0.87 for the MN

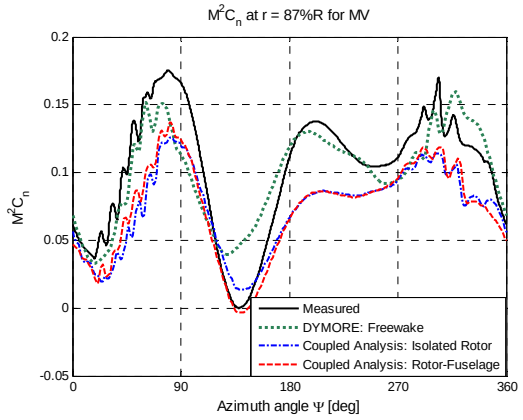

Figure 7 Correlation of M^2C_n at r/R=0.87 for the MV

Trim

The collective, lateral and longitudinal cyclic pitch control angles are adjusted by DYMORE in the coupled analysis to match the measured thrust, hub rolling and pitching moments of which values are given in Ref. [3]. Figure 8 shows the trim iteration history of the loosely-coupled analysis using the rotor-fuselage model for the BL case. As seen in the figure, the thrust and hub moments in KFLOW analysis are converged well through a total of 6 iterations. Table 3 summarizes the trimmed pitch control angles by DYMORE analysis alone with the freewake model and DYMORE/KFLOW coupled analyses using the isolated rotor and rotor-fuselage models for the BL, MN, and MV cases. All of the trimmed pitch control angles are compared well with the measured values. As seen in the table, the lateral and longitudinal cyclic pitch control angles are improved by the coupled analysis with the rotor-fuselage model as compared to the coupled analysis using the isolated rotor model and DYMORE analysis alone.

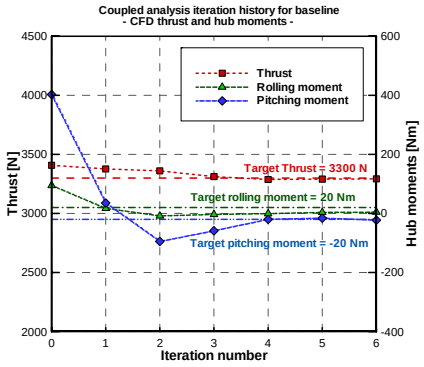

Figure 8 Trim iteration history of the coupled analysis using the rotor-fuselage model for the BL

Table 3 Correlations of trim pitch control angels

Baseline (BL)	θ_0	θ_{1c}	θ_{1s}
Measured	3.80°	1.92°	-1.34°
DYMORE(freewake)	3.81°	1.45°	-1.32°
Coupled analysis(Isolated rotor)	3.82°	1.57°	-0.84°
Coupled analysis(Rotor-fuselage)	3.86°	1.89°	-1.15°
Minimum noise (MN)	θ_0	θ_{1c}	θ_{1s}
Measured	3.91°	2.00°	-1.35°
DYMORE(freewake)	3.98°	1.42°	-1.44°
Coupled analysis(Isolated rotor)	3.91°	1.60°	-0.80°
Coupled analysis(Rotor-fuselage)	4.00°	1.92°	-1.05°
Minimum vibration (MV)	θ_0	θ_{1c}	θ_{1s}
Measured	3.80°	2.01°	-1.51°
DYMORE(freewake)	3.98°	1.46°	-1.43°
Coupled analysis(Isolated rotor)	3.70°	1.51°	-1.00°
Coupled analysis(Rotor-fuselage)	3.80°	1.85°	-1.24°

Blade deformations

Figures 9 to 11 correlate the predictions of the blade flap deflections (w) and elastic torsion deformations (φ) at the tip for the BL, MN, and MV cases with the measured data. The lead-lag deflection correlation is not conducted in this paper since all the previous correlation studies have shown the significant offset from the measured data. The flap deflection was measured without a precone angle, and its positive direction is defined as a flap-up. The elastic

torsion deformation is defined without pitch controls and a pretwist, and the positive direction is defined as a nose-up. Figure 9 shows the correlation of the flap deflection and elastic torsion deformation in the BL. The measured flap deflection shows a slight blade-to-blade variation due to the blade dissimilarity. As appeared in the figure, all the present analyses predict the flap deflection well although the peak-to-peak values are slightly under-predicted. The measured elastic torsion deformation shows a large blade-to-blade variation with a mean value difference of 0.6˚. DYMORE with the freewakes predicts the waveform of the elastic twist deformation reasonably, but its peak-to-peak value is significantly under-predicted. Both the two coupled analyses improve the peak-to-peak value considerably though both the mean values are under-predicted. Furthermore, the rotor-fuselage model improves moderately the phase of the elastic torsion deformation which is closely related to the phase of the section normal force as compared to the result using the isolated rotor model which shows a slight phase lag behavior.

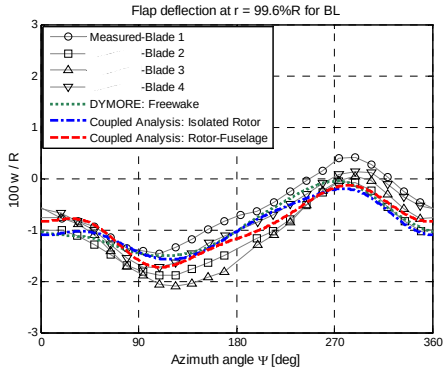

(a) Flap deflection

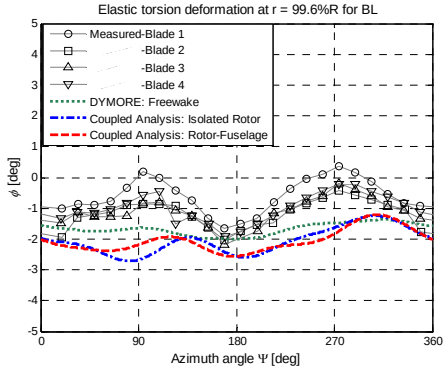

(b) Elastic torsion deformation

Figure 9 Correlation of the blade tip deformations for the BL

Figure 10 predicts the flap deflection and elastic twist deformation at the blade tip for the MN case. As in the result for the BL case, all the predictions of the flap deflection show good correlations. The correlations of the elastic torsion deformation are also nice however both the mean values of the two coupled analyses are moderately under-predicted. In addition, unlike the previous BL case the fuselage model in the coupled analysis does not a significant effect on the elastic torsion deformation in the MN case. This is tightly related to the fact that the fuselage model in the coupled analysis does not a significant effect on the phase of M^2C_n as already observed in Figure 6. The correlations of the blade tip deformations for the MV case are given in Figure 11. The correlation trend is quite similar to that of the MN case. However the coupled analyses show slightly better correlations of the flap deflection at near the azimuth angle of 0˚ as compared to the prediction by DYMORE with the freewake model. The measured elastic torsion deformation shows larger scatter. All the peak-to-peak values of the elastic torsion deformation in the present analyses are moderately under-predicted.

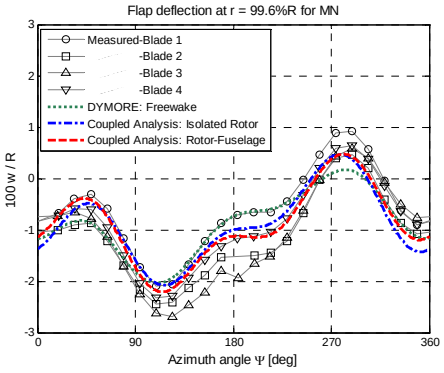

(a) Flap deflection

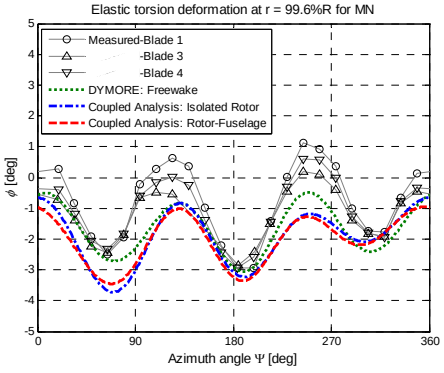

(b) Elastic torsion deformation

Figure 10 Correlation of the blade tip deformations for the MN

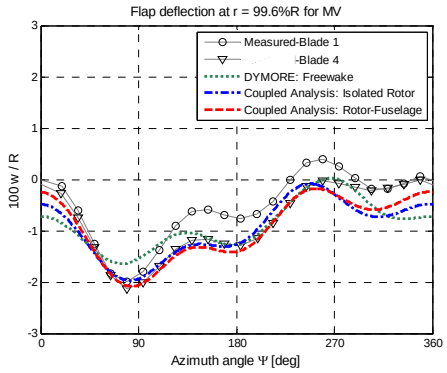

(a) Flap deflection

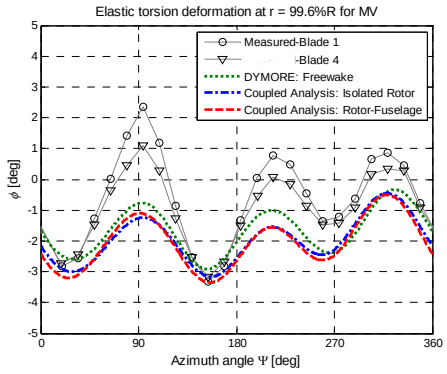

(b) Elastic torsion deformation

Figure 11 Correlation of the blade tip deformations for the MV

Blade structural loads

Figures 12 to 14 correlate the predicted blade structural loads such as the flap bending, lead-lag bending and torsion moments with the measured data [11] for the BL, MN, and MV cases. The flap bending and lead-lag bending moments at r/R=0.17 and torsion moment at r/R=0.33 are considered for the correlation. The positive directions of the flap bending, lead-lag bending, and torsion moments are defined as a bent-up, bent-forward (to the leading edge), and pitch-up, respectively. Since the large offset in the mean values of the blade structural loads is usually observed between the prediction and measurement, the oscillatory loads without the mean values (1-per-rev and higher harmonics) are considered in the present correlation.

Figure 12 correlates the flap bending moments for the BL, MN, and MV cases with the measured data. As seen in the figure, DYMORE with freewakes shows poor predictions for all the three test cases since its peak-to-peak is under-predicted considerably and the waveform is also different from the measured data particularly at around the azimuth angle of 270˚. However the coupled analyses improve the correlation significantly for all the test cases and the results with the isolated rotor and rotor-fuselage models are very close to each other.

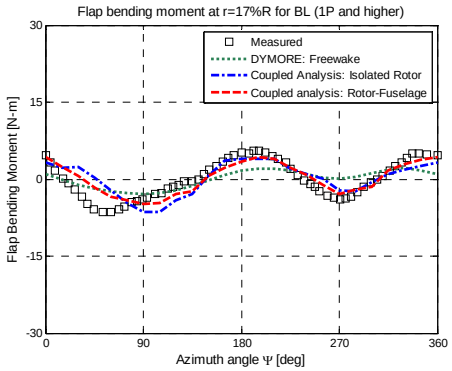

(a) BL

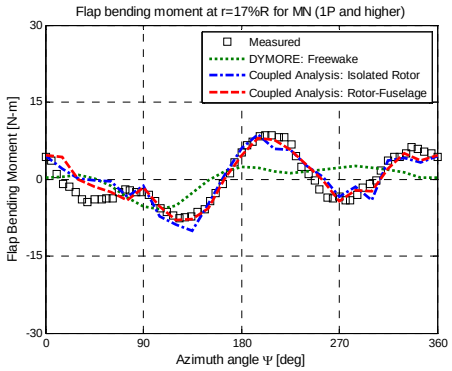

(b) MN

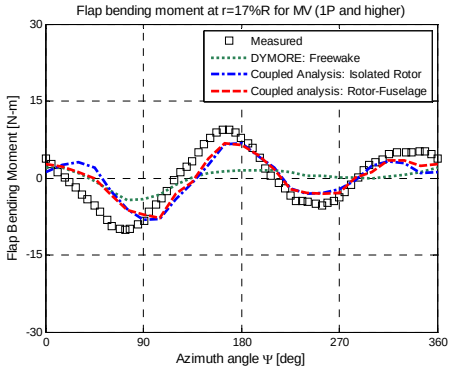

(c) MV

Figure 12 Correlations of the flap bending moment at r/R=0.17

Figure 13 gives the correlations of the lead-lag bending moments for the BL, MN, and MV cases. All of the present predictions capture reasonably the waveform with a one-per-rev but the significant differences at around the azimuth angle of 180˚ are commonly observed.

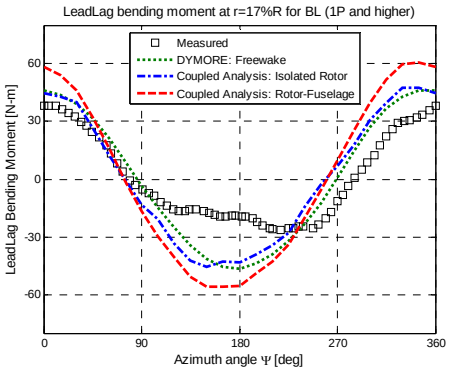

(a) BL

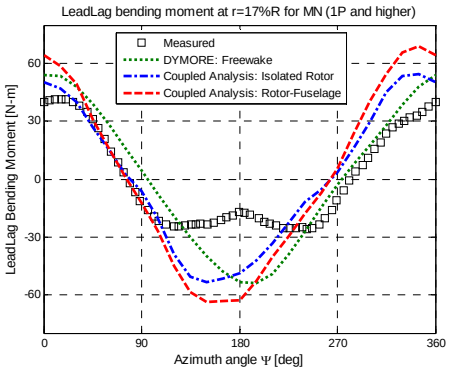

(b) MN

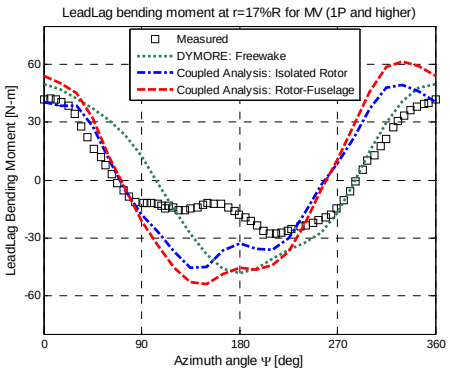

(c) MV

Figure 13 Correlations of the lead-lag bending moment at r/R=0.17

The correlations of the torsion moments for the three test cases are shown in Figure 14. For the BL case, a reasonable correlation is obtained by DYMORE with the freewake model however its peak-to-peak is under-predicted slightly and it does not capture a gentle down-up behavior at the azimuth angle of 90˚. The predictions by the coupled analyses with the isolated rotor and rotor-fuselage models are similar to each other and they improve the correlation significantly since the peak-to-peak value is predicted nicely and the waveform is also correlated well with the measured data although there is the slight phase lag behavior in the fourth quadrant. For the MN case, all the present predictions are correlated well with the measured data but DYMORE with the freewake model shows a better prediction in the fourth quadrant as compared with the two results by the coupled analyses. The coupled analyses using the isolated rotor and rotor-fuselage models give a quite similar prediction to each other. For the MV case, DYMORE analysis alone as well as the coupled analyses shows a good correlation although all the present analyses under-predict the magnitudes in the second and third quadrants. In addition, like the previous correlations the effect of the fuselage model in the coupled analysis is insignificant on the blade structural loads.

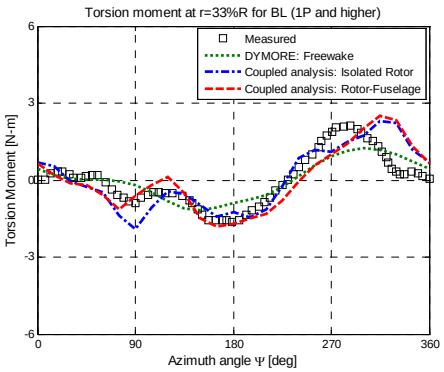

(a) BL

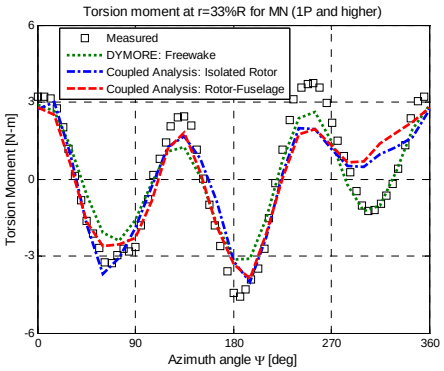

(b) MN

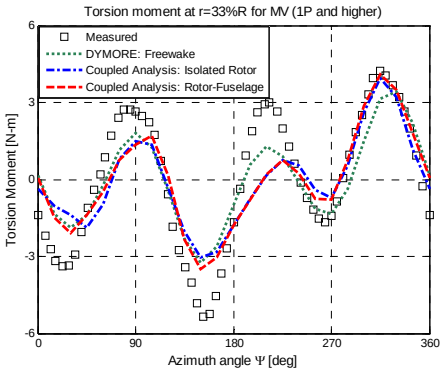

(c) MV

Figure 14 Correlations of the torsion moment at r/R=0.33

Wake positions

Figure 15 shows the location and orientation of the PIV measurement windows for the BL case. In the figure the vortex lines are obtained from freewake predictions [3]. In order to avoid the disturbances of the blade presence and due to the arrangement of the cameras in the HART II test, the wake structure was measured in the first and third quadrants when the reference blade was at the azimuth angle of 20˚ and it was also measured in the second and fourth quadrants when the reference blade was at the azimuth angle of 70˚. The present correlation of the wake positions considers the vortices in the planes at y/R=±0.7R which are at the positions 17-19 and 46-47 for ψ=70˚and the positions 20-23 and 43-35 for ψ=20˚. Figure 16 predicts the wake geometry using the coupled analysis with the rotor-fuselage model for the BL case. The predicted wake geometry is represented by the iso-surfaces of Q-criterion colored by the vorticity magnitude. Red indicates high magnitude in the predicted wake geometry.

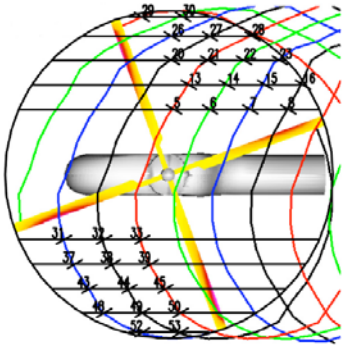

(a) ψ=20˚

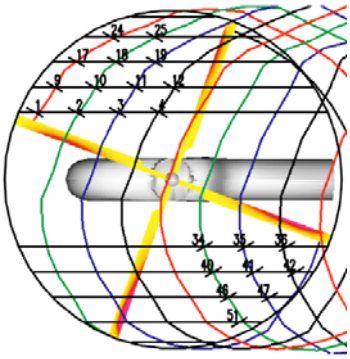

(b) ψ=70˚

Figure 15 PIV measurement positions for the BL [3]

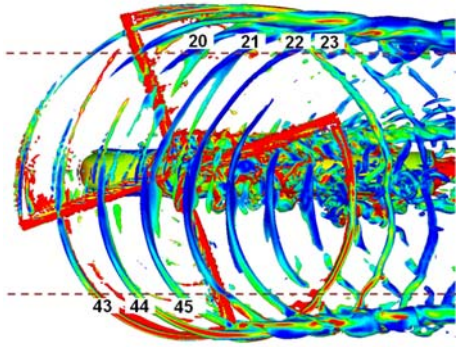

(a) ψ=20˚

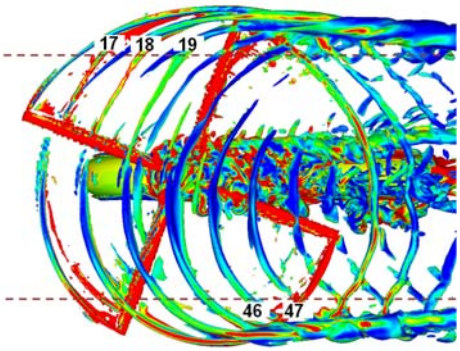

(b) ψ=70˚

Figure 16 Predicted wake geometry for the BL

Figures 17 to 19 correlate the wake positions for the BL, MN, and MV cases against the measured data. The results by the coupled analyses using the isolated rotor and rotor-fuselage models are considered in this correlation. In the hub coordinate system, z_h is positive in the upward direction and x_h is positive aft. For the BL case as shown in Figure 17, both the coupled analyses predict the wake positions (positions 17-19) well when the reference blade was at ψ=70˚ in the advancing side. However the isolated

rotor model under-predicts slightly the wake positions (positions 20-22) in the vertical direction at ψ=20˚ in the advancing side. Both the isolated rotor and rotor-fuselage models predict well the vortex locations in the retreating side.

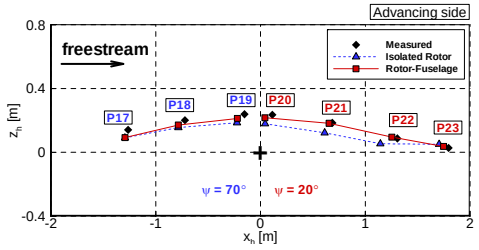

(a) Advancing side

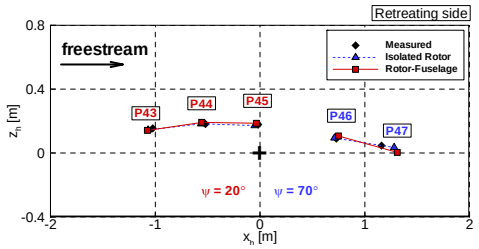

(b) Retreating side

Figure 17 Correlation of the wake positions for the BL

Figure 18 shows the correlation of the wake positions for the MN case. The vortex at position 23 is not considered since its measurement was missed. As given in the figure, the coupled analysis using the isolated rotor model as well as that with the rotor-fuselage model predicts the vortex locations nicely in the advancing side although both the models predict the vortex location of position 22 ahead of the measured location by approximately 1.4*c* in the horizontal direction. But, the coupled analysis with the rotor-fuselage model show a better correlation since it predicts the locations of the vortices in the vertical direction nicely as compared to the result using the isolated rotor model. The predicted vortex locations with both the two models in the retreating side are correlated well with the measured locations.

The comparison of the wake positions for the MV cases is given in Figure 19. The rotor wake structure in the MV case is quite interesting since the dual tip vortices on the advancing side due to the negative loading near the blade tip on the advancing side are observed. On the advancing side with the dual tip vortices, the isolated rotor model predicts the positions of the clockwise and counter-clockwise vortices reasonably but the predicted locations are slightly are lower in the vertical direction than the measured locations. The rotor-fuselage model gives good correlations of the positions of both the clockwise and counter-clockwise vortices with the measured data. The vortices on the retreating side by both the models are also correlated well with the measured locations.

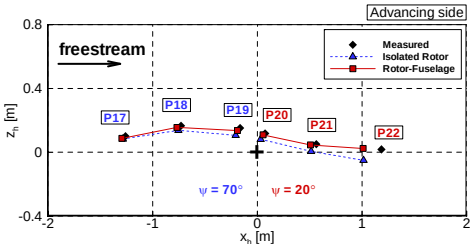

(a) Advancing side

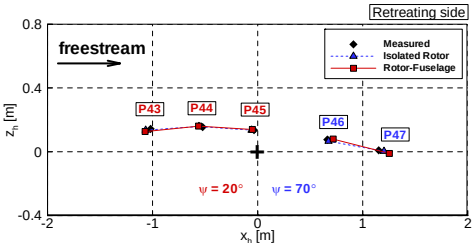

(b) Retreating side

Figure 18 Correlation of the wake positions for the MN

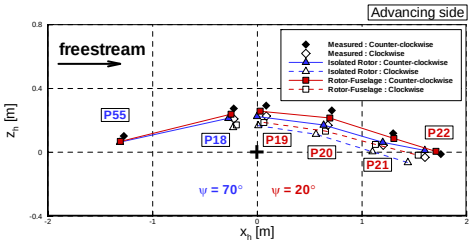

(a) Advancing side

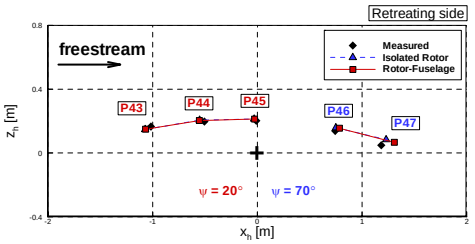

(b) Retreating side

Figure 19 Correlation of the wake positions for the MV

Conclusions

In this work, a loosely-coupled analysis was conducted, using a nonlinear flexible multibody dynamics code DYMORE and a RANS CFD solver KFLOW, to correlate the measured HART II data for the BL, MN, and MV cases. Both a rotor-fuselage model and an isolated rotor model were used. From the present correlation study, the following conclusions were obtained:

1) The present coupled analysis predicted the BVI airloads reasonably well, against the measured data, for the three test cases. A significant improvement of predictions on the phases and the BVI airloads were obtained with a fuselage model, for the BL case. However, no substantial changes were met in both the MN and MV cases.

2) The coupled analysis with a rotor-fuselage model improved the correlation of the trimmed cyclic pitch control angles by 0.2˚ to 0.5˚ for the three test cases consistently, as compared to the coupled analysis with an isolated rotor model and DYMORE analysis alone with a freewake analysis.

3) All the predicted results on elastic deformations showed reasonable correlations against the measured data. Generally, the rotor-fuselage model improved the phase of the elastic twist deformation for the BL case, as compared to that with an isolated rotor model.

4) Both the coupled analyses demonstrated significant improvements on the flap bending moment, as compared with DYMORE analysis alone. The torsion moments predicted using the coupled analyses with an isolated rotor model and a rotor-fuselage model were correlated well with the measured data. All the predicted lead-lag bending moments over-predicted the peak-to-peak magnitudes against the measured data.

5) The predicted vortex positions using the coupled analyses showed good agreements with the measured data. However, the coupled analysis with the rotor-fuselage model showed a better prediction than the result using the isolated rotor model.

Acknowledgements

This research was supported by Leading Foreign Research Institute Recruitment Program through the National Research Foundation of Korea (NRF) funded by the Ministry of Education, Science and technology (MEST) (K2060100001) and by KARI under the Technology Development of Bearingless Main Rotor Hub System funded by the MKE of Korea. The authors would like to thank the HART II team for the test data.

References

[1] Yu, Y.-H., Tung, C., van der Wall, B. G., Pausder, H.-J., Burley, C., Brooks, T., Beaumier, P., Delrieux, Y., Mercker, E., and Pengel, K., "The HART-II test: rotor wakes aeroacoustics with Higher-Harmonic pitch Control (HHC) inputs -The joint German/ French/Dutch/US project-," Proceedings of the American Helicopter Society 58th Annual Forum, 2002.

[2] Yu, Y.-H., Gmelin, B., Heller, H., Phillippe, J. J., Mercker, E., and Preisser, J. S., "HHC aeroacoustics rotor test at the DNW – The joint German/French/US HART project," Proceedings of 20th European Rotorcraft Forum, 1994.

[3] Van der Wall, B. G., "2nd HHC Aeroacoustic rotor test (HART II) - Part II: Representation results-," Institute Report IB 111-2005/03, German Aerospace Center (DLR), Braunschweig, Germany, 2005.

[4] Lim, J.-W. and van der Wall, B. G., "Investigation of the Effect of a Multiple Trailer Wake Model for Descending Flights," Proceedings of the American Helicopter Society 61st Annual Forum, 2005.

[5] Park, J.-S., Jung, S. N., "Comprehensive Multibody Dynamics Analysis for Rotor Aeroemechanics Predictions in Descending Flight," The Aeronautical Journal, Submitted for Review, 2011.

[6] Yang, C.-M., Inada, Y., Aoyama, T., "BVI Noise Prediction using Motion Data," Proceedings of 1st International Forum on Rotorcraft Multidisciplinary Technology, 2007.

[7] Sa, J.-H., Kim, J.-W., Park, S.-H., Park, J.-S., Jung, S. N., Yu, Y.-H., "KFLOW results of airloads on HART-II rotor blades with prescribed blade deformation," Proceedings of 2nd International Forum on Rotorcraft Multidisciplinary Technology, 2009.

[8] Lim, J.-W., Nygaard, T. A., Strawn, R., and Potsdam, M., "BVI airloads prediction using CFD/CSD loose coupling," Proceedings of the American Helicopter Society 4th Vertical Lift Aircraft Design Conference, 2006.

[9] Biedron, R. T., Lee-Rausch, E. M., "Rotor Airloads Prediction Using Unstructured

Meshes and Loose CFD/CSD Coupling," Proceedings of 26th AIAA Applied Aerodynamics Conference, AIAA Paper 2008-7341, 2008.

[10] Boyd, Jr., D. D., "HART II Acoustic Predictions using a Coupled CFD/CSD Method," Proceedings of the American Helicopter Society 65th Annual Forum, 2009.

[11] Lim, J.-W., Dimanlig, A. C. B., "The Effect of Fuselage and Rotor Hub on blade-Vortex Interaction Airloads and Rotor Wakes," Proceedings of 36th European Rotorcraft Forum, Paper No. 051, 2010.

[12] Sa, J.-H., You, Y.-H., Park, J.-S., Jung, S. N., Park, S.-H., Yu, Y.-H., "Assessment of CFD/CSD Coupled Aeroelastic Analysis Solution for HART II Rotor Incorporating Fuselage Effects," Proceedings of the American Helicopter Society 67th Annual Forum, 2011.

[13] Lim, J.-W., Wissink, A., Jayaraman, B., Dimanlig, A., "Application of Adaptive mesh Refinement Technique in Helios to Blade-Vortex Interaction Loading and Rotor Wakes," Proceedings of the American Helicopter Society 67th Annual Forum, 2011.

[14] Lynch, C. E., "Advanced CFD Methods for Wind Turbine Analysis," Ph.D thesis, Georgia Institute of Technology, 2011.

[15] Johnson, W., "CAMRAD II, Comprehensive Analytical Model of Rotorcraft Aerodynamics and Dynamics," Johnson Aeronautics, 1992.

[16] Bauchau, O. A. DYMORE manual: http://soliton.ae.gatech.edu/people/obauchau/Dwnld/dymore20/DymoreManual.pdf.

[17] Anderson, W. K., Bonhaus, D. L., "An Implicit Upward Algorithm for Computing Turbulent Flows on Unstructured Grids," *Computers and Fluids*, 1994, 23(1), pp.1-22.

[18] Van der Wall, B. G., "2nd HHC Aeroacoustic rotor test (HART II) - Part I: Test document-," Institute Report IB 111-2003/31, German Aerospace Center (DLR), Braunschweig, Germany, 2003.

[19] Hodges, D. H., "A Mixed Variational Formulation based on Exact Intrinsic Equations for Dynamics of Moving Beams," *International Journal of Solids and Structures*, 1990, **26**, (11), pp 1253-1273.

[20] Peters, D. A., He, C. J., "Finite State Induced Flow Models Part II: Three-Dimensional Rotor Disk," *Journal of Aircraft*, 1995, **32,** (2) pp 323-333.

[21] Bhagwat, M. J., Leishman, J. G., "Stability, Consistency and Convergence of Time-Marching Free-Vortex Rotor Wake Algorithms," *Journal of the American Helicopter Society*, 2001, **46**, (1), pp 59-71.

[22] Potsdam, M., Yeo, H., Johnson, W., "Rotor airloads prediction using loose aerodynamic/ structural coupling," Proceedings of the American Helicopter Society 60th Annual Forum, 2002.